



An observation of primary production enhanced by coastal upwelling in the southwest East/Japan Sea



Doshik Hahm^{a,*}, Tae Siek Rhee^b, Hyun-Cheol Kim^c, Chan Joo Jang^d, Yong Sun Kim^d, Jae-Hun Park^e

^a Department of Oceanography, Pusan National University, Busan 46241, South Korea

^b Division of Polar Ocean Sciences, Korea Polar Research Institute, Incheon 21990, South Korea

^c Unit of Arctic Sea-Ice Prediction, Korea Polar Research Institute, Incheon 21990, South Korea

^d Ocean Circulation and Climate Research Division, Korea Institute of Ocean Science & Technology, Busan 49111, South Korea

^e Department of Ocean Science, Inha University, Incheon 22212, South Korea

ARTICLE INFO

Keywords:

Coastal upwelling
Primary production
East Sea
O₂/Ar

ABSTRACT

Coastal upwelling (CU) is an important process that causes changes in physical and chemical properties, resulting in variation of biological processes in a coastal area. In the southwestern part of the East/Japan Sea (SWES), CU has been alleged as one of the mechanisms responsible for higher net primary production (NPP) than the rest of the East/Japan Sea. We provide, for the first time, high spatial resolution underway observations of sea surface temperature, salinity, chlorophyll-*a* fluorescence and $\Delta(\text{O}_2/\text{Ar})$, revealing the physical and biological characteristics of the upwelled waters in the SWES. The cold, upwelled waters retained high fluorescence and $\Delta(\text{O}_2/\text{Ar})$, consistent with enhanced phytoplankton biomass and biological O₂ production by CU. The net community production (NCP) in the ambient and upwelled waters were 33 ± 19 and 77 ± 41 mmol O₂ m⁻² d⁻¹, respectively. The latter should be considered as a lower bound, containing a significant fraction of low O₂ waters from subsurface. Satellite observation indicated that NPP in the upwelled waters were higher than the ambient waters by 51%. This implies that up to half of higher NPP in the SWES than the rest of the East/Japan Sea can be ascribed to CU events.

1. Introduction

Coastal upwelling (CU) is an important process that causes changes in physical and chemical properties in the upper water column, resulting in variation of biological processes in a coastal area (Bakun, 1990; Capone and Hutchins, 2013). CU results from the winds blowing along a coast that transport surface water offshore. The transport of the surface water pulls cooler subsurface water toward the surface regions along the coast. Because the upwelled water is rich in nutrients, the CU often results in enhanced primary production in nutrient-limited regions (Lachkar and Gruber, 2013; Capone and Hutchins, 2013).

In the East/Japan Sea, a marginal sea in the Northwest Pacific, the southwestern part is a well-known place of CU. Because the coastline of the Korean peninsula runs roughly south-to-north direction, CU occurs typically in summer when southerly winds blow over the coast, notably near Gampo-Ulgi region (Fig. 1; Lee, 1983; Lee and Na, 1985). It is known that the upwelling center is within < 20 km from the coast and that the upwelled water is confined to surface layer in the off-center

region (Lee and Na, 1985; Byun, 1989). The upwelled, cold water is transported offshore by the East Korean Warm Current and Ulleung Warm Eddy (UWE; Chang et al., 2004; Hyun et al., 2009).

Among the three basins of the East/Japan Sea, namely, the Japan, Yamato, and Ulleung Basins (UB), the UB in the southwest of the East Sea (SWES) exhibits significantly higher net primary production (NPP) than other basins. For example, Yamada et al. (2005) reported annual NPP of 222 gC m⁻² y⁻¹ in the UB, higher than those of the Japan Basin (161 gC m⁻² y⁻¹) and the Yamato Basin (191 gC m⁻² y⁻¹) based on SeaWiFS chlorophyll *a* (Chl-*a*) observations. More recently, Joo et al. (2014) reported even higher annual NPP in the UB of 280 gC m⁻² y⁻¹, based on MODIS-derived primary production. The *in situ* observations by Kwak et al. (2013a) also showed that summer NPP rates of 0.37–0.96 gC m⁻² d⁻¹ in the UB was much higher than those in the East China and the Western Pacific Ocean (0.17–0.28 gC m⁻² d⁻¹).

It appears that several processes may be responsible for the higher annual and summer NPP in the SWES. Some (Onitsuka et al., 2007; Kim et al., 2013) argued nitrogen transported by Tsushima Warm Current

* Corresponding author.

E-mail address: hahm@pusan.ac.kr (D. Hahm).

<https://doi.org/10.1016/j.jmarsys.2019.03.005>

Received 28 August 2018; Received in revised form 30 January 2019; Accepted 22 March 2019

Available online 28 March 2019

0924-7963/ © 2019 Elsevier B.V. All rights reserved.

(TWC), influencing mainly on the SWES, is responsible for the higher NPP. Kwak et al. (2013a) further suggested that the pycnocline of TWC shallows as it flows over the continental shelves and the shoaling allows for nutrients immediately below pycnocline to be supplied to the surface. Others suggested that CU (Onitsuka et al., 2007; Hyun et al., 2009; Yoo and Park, 2009) is an important mechanism providing subsurface nutrients to surface layers. Yet others suggested that UWEs not only carry inshore upwelled waters to offshore but also support substantial biomass in the SWES, by mixing nutrient-depleted surface waters with deep waters (Hyun et al., 2009; Kim et al., 2012).

A limited number of studies reported biological consequence of the CU. Hyun et al. (2009) observed that biomass and production were higher in the ring of a UWE than in the core or outside of the eddy and that diatom species composition and physico-chemical parameters of the ring were similar to those of upwelled waters near the coast. These observations led them to argue that anticyclonic eddies in the UB entrain productive upwelled waters and deliver high production to the basin. Yoo and Park (2009) showed a strong correlation between Chl-*a* variations of the CU regions and of the SWES using satellite data from 1998 to 2006. They further suggested that the high production in the SWES is enhanced mainly by CU occurring along the southeastern coast of Korea.

Although the above studies showed an increase in phytoplankton biomass, none of them have quantified *in situ* production enhanced by CU. This is largely due to the fact that classical on-deck incubation is not an efficient method to capture the spatial scale (200–300 km) and relatively short duration (several weeks) of the CU. To the contrary, high-frequency measurements of $\Delta(O_2/Ar)$ by mass spectrometry (Tortell, 2005; Cassar et al., 2009) provide an opportunity to investigate net community production (NCP), defined as the difference between NPP and heterotrophic respiration, with a high spatial resolution (< 1 km). Compared to the on-deck incubation method, such high-resolution O_2/Ar measurements can be considered as a real-time tool to map spatial variability of biological productivity. Here, we provide the first underway NCP measurements based on O_2/Ar method, capturing the physical and biogeochemical nature of the upwelled and ambient waters in the SWES (Fig. 1). The observations and satellite data were used to quantify increases of Chl-*a* and NPP in the SWES.

2. Methods and data

2.1. The underway measurements

Underway observations were carried out during an annual test cruise of IBRV Araon from 17 to 25 July 2013. Seawater at a nominal depth of 7 m was pumped into the laboratory and measured for sea surface temperature (SST) and salinity (SSS) using a thermosalinograph (SBE 45). Chl-*a* fluorescence, a proxy of Chl-*a* biomass, was measured using a Turner Designs 10-AU equipped with a continuous flow cuvette.

The concentrations of dissolved oxygen were measured using an oxygen optode (AAndera 3835). Salinity compensation was applied to the raw values according to the manufacturer's operation manual and then gain correction was applied further. The gain was determined after the cruise by measuring oxygen in the air with known atmospheric temperature and pressure (Johnson et al., 2015). A comparison between optode and Winkler titration measurements carried out in a separate cruise suggested that after the salinity and gain correction optode concentrations differ from titration values by $< 2\%$.

The ratios of O_2/Ar were measured using the equilibrator inlet mass spectrometry system (Cassar et al., 2009) described in Hahn et al. (2014). Surface water pumped into the laboratory was equilibrated in a Weiss-type equilibrator. The O_2/Ar of the equilibrated air was measured in a quadrupole mass spectrometer and calibrated every 3 h against the O_2/Ar of marine air from the foremast.

Juranek et al. (2010) reported that O_2 concentration could be reduced by respiration in underway seawater lines by up to 2%. Because

no comparison was made between O_2 concentrations in seawaters from the underway line and from Niskin bottles, it is not clear if the underway line of IBRV Araon was suffered from the respiration problem or not. If so, our O_2/Ar observation and thus NCP estimates were likely to be underestimated by 2%.

2.2. Calculation of NCP from O_2 and Ar measurements

Dissolved oxygen concentration in the mixed layer is the sum of the O_2 derived from biological (respiration and photosynthesis) and physical (dissolution of air, bubble injection, and changes in water temperature and air pressure) processes. Because Ar is biologically inert and has solubility and diffusivity similar to those of O_2 , the amount of biologically derived O_2 can be isolated by measuring the O_2/Ar ratio (Craig and Hayward, 1987; Spitzer and Jenkins, 1989). The biological O_2 , $[O_2]_{bio}$, is defined as:

$$[O_2]_{bio} = [O_2] - [O_2]_{phys} = \Delta(O_2/Ar) \cdot [O_2]_{sat} \cdot [Ar]/[Ar]_{sat}, \quad (1)$$

$$\text{where } \Delta(O_2/Ar) = [(O_2/Ar)_{sample}/(O_2/Ar)_{sat} - 1] \quad (2)$$

$(O_2/Ar)_{sample}$ and $(O_2/Ar)_{sat}$ are O_2/Ar ratios of samples and air-saturated waters, respectively. Neglecting vertical mixing, often the case in the open ocean, O_2/Ar ratios in the mixed layer primarily reflect the balance between NCP (in units of $\text{mmol } O_2 \text{ m}^{-2} \text{ d}^{-1}$) and gas exchange of $[O_2]_{bio}$:

$$NCP = k_w \cdot [O_2]_{bio} = k_w \cdot \rho \cdot [O_2]_{sat} \cdot \Delta(O_2/Ar), \quad (3)$$

where k_w and $[O_2]_{sat}$ is the weighted gas transfer velocity and air-saturated concentration of O_2 , respectively. ρ is density of the surface water. In the above equation, $[Ar]/[Ar]_{sat}$ was assumed to be 1. It is noted that Manning et al. (2017) who conducted $[Ar]$ measurements in Monterey Bay reported average $[Ar]/[Ar]_{sat}$ of 1.036. The assumption of $[Ar]/[Ar]_{sat} = 1$ may introduce an error of 3.6% into NCP estimates.

k_w is a weighted average of instantaneous gas transfer velocities (k) of the past days (Eq. (6) of Reuer et al., 2007), adopted to account for $\Delta(O_2/Ar)$ dependency on prior wind speeds at the observation time. Due to a relatively shorter O_2 residence time in the mixed layers, largely resulting from shallow mixed layers in summer (~ 12 m; Lim et al., 2012), the influence of winds 20–30 days prior the observation became insignificant in the summer SWES. To account for this, adopted were a shorter weighting interval of 30 days and the weighting scheme modified for shorter time intervals of Teeter et al. (2018). k values were calculated 4 times a day from NCEP 6-hourly wind speeds at 10 m above the sea surface (Kalnay et al., 1996) and the parameterization of Wanninkhof (1992). The k and climatological mixed layer depths (MLDs) of Lim et al. (2012) with a horizontal resolution of $0.5^\circ \times 0.5^\circ$ were used to calculate k_w . The MLD dataset compiled temperature profiles from 1931 to 2005, including World Ocean Data Base 2005 (Boyer et al., 2006) and recent observations using ships and profiling floats. The O_2 and Ar solubilities were determined according to Garcia and Gordon (1992) and Hamme and Emerson (2004), respectively. Whenever necessary, we adopted a factor of $0.00857 \text{ g C m}^{-2} \text{ d}^{-1} / \text{mmol } O_2 \text{ m}^{-2} \text{ d}^{-1}$ to convert NCP units, assuming a photosynthetic quotient of 1.4 for new production (Laws, 1991).

It is acknowledged that 'negligible vertical mixing' assumed above can be problematic, especially in upwelling regions where a significant influence of subsurface waters is expected. Although there is an attempt to assess the influence of upwelling on NCP (e.g., Haskell et al., 2017), the lack of vertical sampling during the observation did not allow a quantitative analysis of the effect of subsurface waters. By comparing a 2-D cross shelf model with underway O_2/Ar measurements near Vancouver Island, Teeter et al. (2018) demonstrated that O_2/Ar -method underestimated NCP significantly near the upwelling zone. This indicates that NCP estimates in the CU region in this study should be considered as a lower bound of the true NCP in the region.

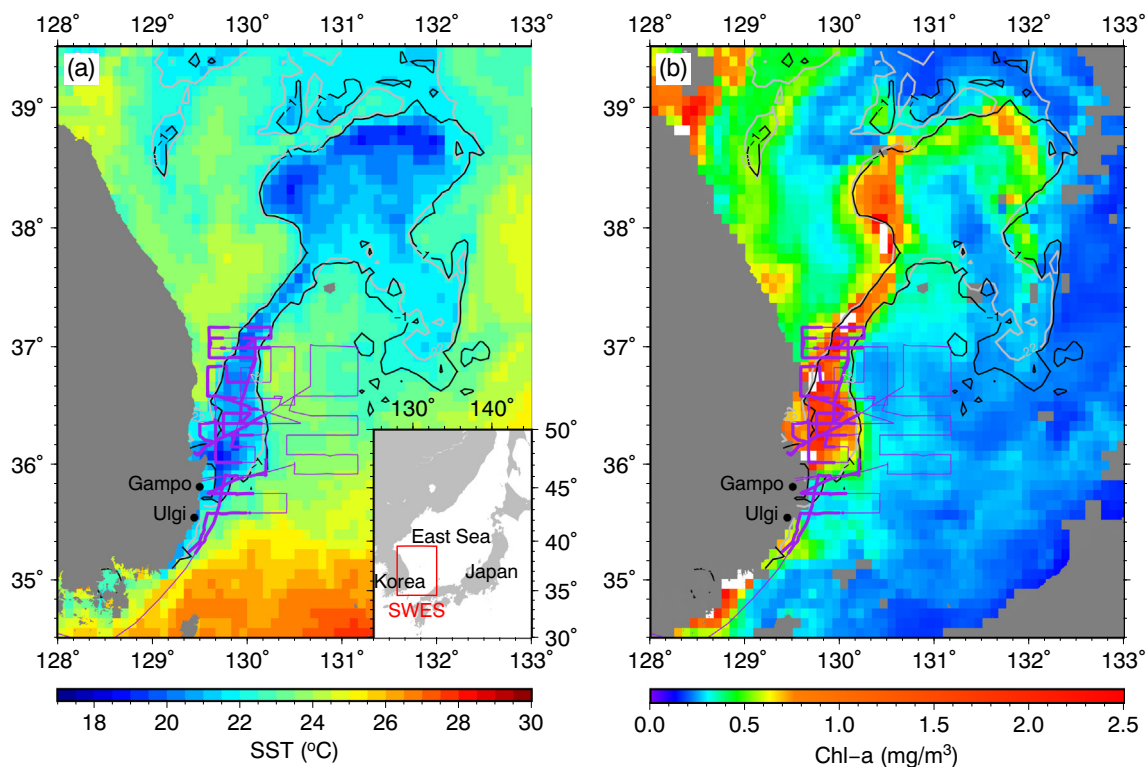


Fig. 1. MODIS-Aqua images of sea surface temperature and Chl-*a* in the SWES in the period between July 20 to 27, 2013. The cold, upwelled waters appeared within the black contour lines of adjusted temperature anomalies $< -1^{\circ}\text{C}$ (see Section 3.4 for details). A substantial increase of Chl-*a* was observed along the path of upwelled waters. The 22°C -isotherms (gray contour lines) overlap with the adjusted temperature anomalies $< -1^{\circ}\text{C}$.

2.3. Satellite data

For comparison with the *in situ* data, we used MODIS-Aqua satellite-derived maps of SST, Chl-*a* (<https://oceandata.sci.gsfc.nasa.gov>) and NPP based on Vertically Generalized Production Model (VGPM-NPP; Behrenfeld and Falkowski, 1997) available at the Ocean Productivity site at Oregon State University. The maps had temporal and spatial resolutions of 8-day and 0.083° by 0.083° , respectively. Those were composites of the images from July 20 to 28, 2013 (between days of year 201 and 208), which mostly overlapped with our *in situ* observations between July 18 to 25, 2013. To facilitate comparison, *in situ* measurements of SST, Chl-*a* fluorescence, and NCP were averaged into the same grids of satellite data (0.083° by 0.083°).

3. Results and discussion

3.1. Underway observations

The SST and SSS along the ship track exhibited significant variations in the range of $13\text{--}25^{\circ}\text{C}$ and $32\text{--}34$, respectively (Fig. 2a and b). The cold waters, with SST less than the mean of 22°C , appeared to carry higher salinity than the surrounding warm waters. The cold, saline waters were ascribed to CU, which is supported by prevailing southerly winds in July along the southeastern coast of the Korean peninsula (Fig. S1). Additionally, warm and saline water masses with temperature of around 24°C and salinity of 33.5 was encountered on 21, 23–24 of July (mostly at east of $130^{\circ}30'\text{E}$). The increases of Chl-*a* fluorescence (a proxy for phytoplankton biomass) were well matched with the appearance of the cold and saline waters, manifested in two broad peaks between 22 and 23 of July (Fig. 2c).

The biological O_2 supersaturation, $\Delta(\text{O}_2/\text{Ar})$, displayed a significant variation during the observation, ranging from -0.1 to 29% (Fig. 2d). The overall positive values indicated that the SWES was in autotrophic environments. The large increases of $\Delta(\text{O}_2/\text{Ar})$ were accompanied with

the increases of Chl-*a* fluorescence (> 0.5), indicating that the higher biological activity, indeed, is responsible for the increased $\Delta(\text{O}_2/\text{Ar})$. The O_2 supersaturation, $\Delta\text{O}_2 = ([\text{O}_2]_{\text{sample}} / [\text{O}_2]_{\text{sat}} - 1) \times 100$, derived from the O_2 optode measurements largely overlapped with large peaks of $\Delta(\text{O}_2/\text{Ar})$, suggesting much of it is due to biological production.

An exceptional discrepancy between $\Delta(\text{O}_2/\text{Ar})$ and ΔO_2 was found at the period of P3 (Fig. 2); ΔO_2 of 24% around midnight of July 22 was almost twice that of $\Delta(\text{O}_2/\text{Ar})$ of 13%. Unlike $\Delta(\text{O}_2/\text{Ar})$, which shows virtually no change by physical processes, ΔO_2 may reflect O_2 change by physical and biological processes. Thus the difference of 11% between ΔO_2 and $\Delta(\text{O}_2/\text{Ar})$ should be ascribed to physical processes such as bubble injection, increase of atmospheric pressure, and warming. Given the fact that supersaturation due to bubble injection or change of atmospheric pressure is usually several percent, we suspect that warming of the upwelled water should be an important physical process responsible for the O_2 supersaturation. For example, about 3°C warming from 10 to 13°C could explain half of the excess (around 6%), assuming no significant air-sea gas exchange in the meantime. The difference might also be caused by dissolution of air bubbles within the underway seawater line under high pressure. However, given the fact that there was no significant ship motion even during the relatively strong winds on July 24 (Fig. 2e), it is less likely that bubbles were involved in the line in a significant amount. It is noted that no air bubble was observed in seawater supplied to the laboratory during the observation period.

The calculated sea-to-air fluxes of $[\text{O}_2]_{\text{bio}}$, calculated with the weighted gas transfer velocities (k_w ; Fig. 2e), largely followed the pattern shared with Chl-*a* fluorescence and $\Delta(\text{O}_2/\text{Ar})$ (Fig. 2f). The high flux on July 24, which were not accompanied by the cold and saline waters, can be attributed to the combined effect of modest $\Delta(\text{O}_2/\text{Ar})$ and much higher k_w on that day ($> 25\text{ cm h}^{-1}$). The k_w was around twice higher than the other days of $\sim 15\text{ cm h}^{-1}$.

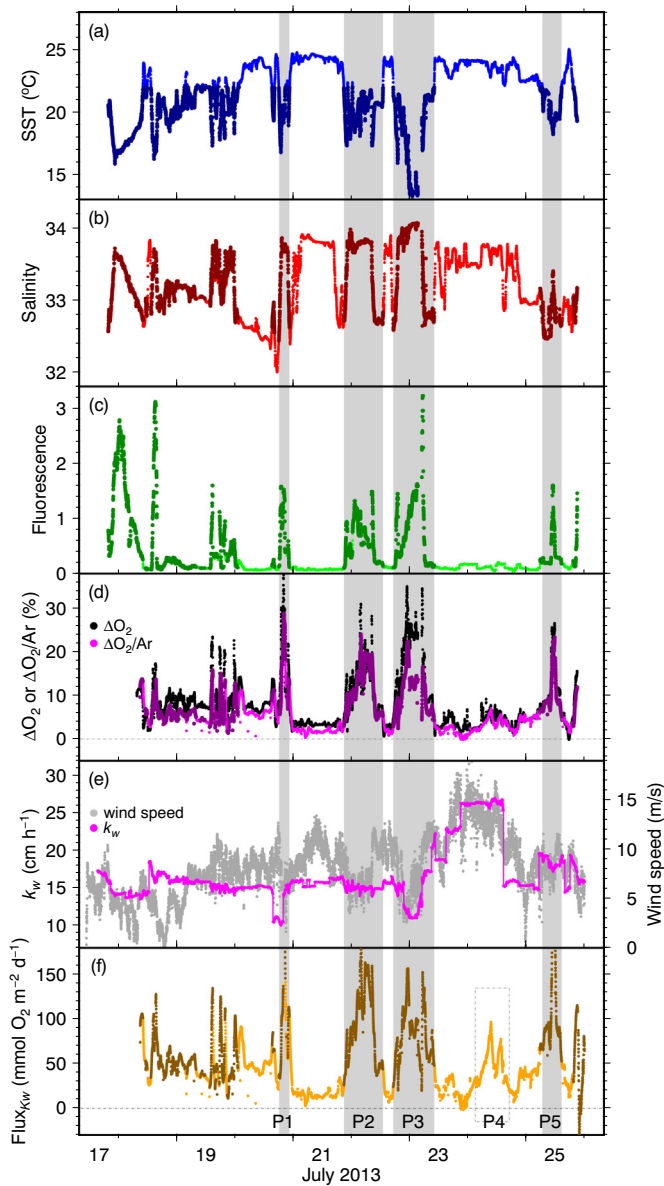


Fig. 2. Variation of surface water properties along the ship track. The light and dark symbols of each parameter indicate the values of the ambient and upwelled waters (temperature < 22 °C), respectively (a–d). Weighted gas transfer velocities (k_w) are shown in panel e, together with wind speeds measured on the ship. $[O_2]_{bio}$ flux calculated with k_w are shown in panel f. The gray shades denote periods of prominent peaks of the flux, accompanied with cold waters. The high flux in the dotted rectangle in July 24 (“P4”) is accompanied with high wind speed and resultant high k_w rather than an apparent cold water.

3.2. Characteristics of the upwelled and ambient waters

The upwelled waters in the observed area was defined simply as the waters with SST lower than the mean of the observed values, 22 °C. The 22 °C-isotherm captures not only the increases of Chl-*a* fluorescence and $\Delta(O_2/Ar)$ of the *in situ* measurements reasonably well (Fig. 2c and d) but also most of significant increases in Chl-*a* (> 0.5 mg m⁻³) in the satellite image (gray contours in Fig. 1b). According to this criterion of < 22 °C, the *in situ* observed areas were divided into 46% of the upwelled and 54% of ambient waters. The upwelled waters defined with the temperature criterion is largely overlapped with those defined with the ‘adjusted SST anomaly’ < -1 °C, which will be discussed in the following section.

Table 1 summarizes the water properties of upwelled and ambient

Table 1

Water properties (average \pm standard deviation) of the upwelled and ambient waters.

	Upwelled (n = 5240)	Ambient (n = 6242)
SST (°C)	19.7 \pm 1.8	23.6 \pm 0.8
Salinity	33.2 \pm 0.4	33.2 \pm 0.5
Chl- <i>a</i> fluorescence	0.64 \pm 0.64	0.11 \pm 0.06
$\Delta O_2/Ar$ (%)	9.3 \pm 5.0	3.6 \pm 2.3
NCP (mmol O ₂ m ⁻² d ⁻¹)	> 77 \pm 41 ^a	33 \pm 19

^a Lower bound of NCP. See Section 3.2 for the explanation.

waters. The mean SST of the upwelled waters was 4 °C lower than that of the ambient waters (*t*-test: $p < 0.05$). The salinity of upwelled waters was virtually identical to that of ambient waters. This was largely due to the presence of the saline (and warm) waters in the eastern part of the survey area. The average fluorescence of 0.64 \pm 0.64 (average and standard deviation) of the upwelled waters was significantly higher than 0.11 \pm 0.06 of the ambient waters (*t*-test: $p < 0.05$). Similarly, $\Delta(O_2/Ar)$ of upwelled waters was nearly three times higher (9.3% \pm 5.0%) than that of ambient waters (3.6% \pm 2.3%) (*t*-test: $p < 0.05$).

Although the higher $\Delta(O_2/Ar)$ and $[O_2]_{bio}$ fluxes (Fig. 2f; Table 1) in the upwelled waters demonstrate qualitatively that the CU process enhances the primary production in the SWES, it is difficult to derive quantitative estimates of NCP in the upwelled waters. As mentioned in the method section, O_2/Ar -NCP method assumes that there is no significant vertical mixing between the mixed and subsurface layers. However, previous studies suggest a significant input of deep, low O_2 waters to the mixed layer in an upwelling region, resulting in underestimation of NCP in the mixed layer (Manning et al., 2017; Teeter et al., 2018). This upward flux of low O_2 waters is likely to be most significant at upwelling centers, usually near coast (< 20 km; Lee and Na, 1985; Byun, 1989) in the SWES.

In the off-center region, cold, upwelled waters are confined to surface layer (Lee and Na, 1985; Byun, 1989) and thus the upward flux of low O_2 waters is not likely to be as significant as that in the upwelling centers. However, this fact alone does not validate NCP estimates in the waters. Typical MLDs of ~ 12 m and k_w of ~ 17 cm h⁻¹ indicate that residence time of O_2 (MLD divided by k_w ; Emerson and Hedges, 2008) should be ~ 3 days in summer SWES. Considering the upwelling of cold waters and their advection to offshore take places in a time scale from several days to weeks, some of the recently upwelled waters may not have enough time to erase the “memory” of low O_2 waters and to reflect NCP in the mixed layer. In this respect, the average NCP of 77 \pm 41 mmol O₂ m⁻² d⁻¹ (Table 1) should be considered as a lower bound of the true NCP (Teeter et al., 2018).

3.3. NCP estimates for the ambient waters

The average NCP of 33 \pm 19 mmol O₂ m⁻² d⁻¹ for the ambient waters were estimated by applying Eq. (3). Because the equation does not include horizontal advection or vertical mixing term, we adopted the approach of Giesbrecht et al. (2012) to estimate potential variation of $[O_2]_{bio}$ flux ($F_{[O_2]_{bio}}$) due to horizontal advection:

$$F_{[O_2]_{bio}} = -v \cdot h \cdot \rho \cdot [O_2]_{bio} / dx \cdot \rho$$

where, v , h , and ρ is current speed, MLD, and density, respectively. Typical values in the ambient waters of 0.15 m s⁻¹ (Lee and Niiler, 2010; Fig. 5), 12 m, 1026 kg m⁻³ were used for the calculation. The horizontal gradient of $[O_2]_{bio}$, $d[O_2]_{bio}/dx$, was estimated to be 7×10^{-5} $\mu\text{mol kg}^{-1} \text{m}^{-1}$ on average, based on our underway $\Delta O_2/Ar$ observations. For the calculation, $[O_2]_{bio}$ were put into grids of 0.083° by 0.083° and spatial gradients were calculated for every pair of the grid points in the ambient waters. Unlike Giesbrecht et al. (2012) who used dO_2/dx to estimated O_2 flux by horizontal advection, we used d

$[O_2]_{bio}/dx$ instead. This way we could tell the $[O_2]_{bio}$ flux only without involving O_2 flux by physical processes. The estimated horizontal flux of $\sim 11 \text{ mmol } O_2 \text{ m}^{-2} \text{ d}^{-1}$ was about 33% of the average gas exchange flux of $[O_2]_{bio}$ (i.e., NCP) for the ambient waters. Because the horizontal gradient of $[O_2]_{bio}$ and the direction of surface currents do not always align each other, the estimated flux should be considered as an upper limit. In short, the maximum uncertainty due to horizontal advection is likely to be 33% of the average NCP for the ambient waters.

Giesbrecht et al. (2012) reported diapycnal mixing between surface and subsurface layers could influence significantly on O_2/Ar mass balance in the mixed layer when subsurface O_2 maximum was present. In summer UB, Rho et al. (2012) observed prevailing subsurface O_2 maxima, indicating that that diapycnal mixing may provide non-trivial upward flux of $[O_2]_{bio}$. If this vertical flux is indeed significant, the average estimate of $33 \text{ mmol } O_2 \text{ m}^{-2} \text{ d}^{-1}$ should reflect not only the NCP in the surface mixed layer but also a fraction of NCP below the mixed layer (Haskell et al., 2016). To quantify NCPs below mixed layer and their contribution to the overall NCPs, it is necessary to observe vertical distribution of $\Delta(O_2/Ar)$ and vertical diffusivity in the future.

The average NCP of $33 \pm 19 \text{ mmol } O_2 \text{ m}^{-2} \text{ d}^{-1}$ in the ambient waters is comparable with those from subtropic-subarctic transition zone and subarctic northeast Pacific of $11\text{--}26 \text{ mmol } O_2 \text{ m}^{-2} \text{ d}^{-1}$ using O_2/Ar method (Lockwood et al., 2012). No previous O_2/Ar -NCP measurements are present in the UB. Instead, Kwak et al. (2013a) reported new production (NP) based on ^{15}N incubation method. Their NP estimates were $0.21 \pm 0.11 \text{ g C m}^{-2} \text{ d}^{-1}$ ($n = 5$) for 6–14 August 2008. Additionally, Kwak et al. (2013b) reported NP estimates of 0.39 and $0.33 \text{ g C m}^{-2} \text{ d}^{-1}$ ($n = 3$) for July and August 2010. In spite of the different method and sampling times, their NP estimates are comparable with our mean NCP of $33 \pm 19 \text{ mmol } O_2 \text{ m}^{-2} \text{ d}^{-1}$, equivalent to $0.28 \pm 0.16 \text{ g C m}^{-2} \text{ d}^{-1}$.

3.4. Enhancement of NPP by CU and NCP-NPP relationships

Because of the presumed non-trivial upward fluxes of subsurface O_2 and lack of vertical observation of $\Delta(O_2/Ar)$, we were only able to provide a lower bound of NCP enhanced by the CU in the upwelled waters. Instead of NCP, we attempted to quantify the increase of NPP in the upwelled waters by adopting satellite based estimates available at the ‘Ocean Productivity’ site. To check if satellite data are consistent with our *in situ* observations, the *in situ* data of SST, Chl-*a*, and NCP were put into grids of 0.083° by 0.083° , matching the grid size of satellite data. Considering different temporal (instantaneous vs. 8-day average) and spatial (spot vs. 0.083° by 0.083°) scales between *in situ* and satellite observations, both datasets displayed reasonably good agreements each other with the correlation coefficients of 0.6–0.7 (Fig. S2).

In order to define ‘upwelled’ water objectively from satellite SST images, we first derived the map of long-term SST by averaging the MODIS images between year 2003 and 2017 for the days of each year between 201 and 208 (Fig. 3a). Next, a map of SST anomaly was derived by subtracting the map of the long-term SST from the 8-day SST map for the days from July 20 to 28, 2013 (Fig. 3c and b). The anomaly map masks out inherent latitudinal SST gradients in the SWES. The map could have provided a way to identify cold waters if the mean of the SST map was the same as that of the long-term SST. For example, one may consider ‘upwelled’ waters are present at the places where SST anomalies are negative. However, if the mean of a SST map is substantial higher/lower than that of the long-term SST due to inter-annual variation caused by large scale air pressure distribution (Park and Kim, 2010), the area of upwelled waters can be under-/over-estimated. To overcome this limitation, we made an adjustment to the SST anomaly maps by further subtracting the difference of the mean of the SST map for the days from July 20 to 28, 2013 and that of the long-term SST map. Finally, the ‘upwelled’ waters are defined as the waters with adjusted SST anomaly $< -1^\circ\text{C}$ (Fig. 3d). Here, -1°C is an approximation

of standard deviations of the adjusted SST anomaly map of the SWES.

Table 2 summarizes the means and standard deviations of gridded *in situ* and satellite data in the upwelled and ambient waters. To expand our analysis from the *in situ* observed area to the SWES, the above mentioned criterion (adjusted SST anomaly $< -1^\circ\text{C}$) was applied for the separation of the two waters. Satellite SST values both in upwelled and ambient waters were $\sim 1^\circ\text{C}$ higher than the gridded *in situ* values; this discrepancy appears to be small given that the area where *in situ* observation was made is $< 16\%$ of the SWES represented by the satellite data. Both *in situ* and satellite Chl-*a* values in the upwelled waters were statistically significantly higher than those in the ambient waters (*t*-test: $p < 0.05$).

Both the gridded fluxes of $[O_2]_{bio}$ and satellite NPP appeared high along the path of the upwelled waters and most of which were found within the adjusted SST anomaly $< -1^\circ\text{C}$ (Fig. 4). The gridded fluxes of $[O_2]_{bio}$, equivalent to NCP, were reported in $\text{g C m}^{-2} \text{ d}^{-1}$, assuming a photosynthetic quotient of 1.4 for NP (Laws, 1991). The upwelled waters had NPP of $1.25 \pm 0.62 \text{ g C m}^{-2} \text{ d}^{-1}$, 51% higher than that of the ambient waters. Considered that the upwelled waters have occupied 20% ($= 560 / (560 + 2286)$; Table 2) of the SWES, the overall NPP increase due to the coastal upwelling was around 10% ($= 51\% \times 0.20$) in the SWES.

Yoo and Park (2009) argued that CU is frequent in all seasons except winter. If it is assumed that CU events, equivalent to the one observed in this study in terms of area and production enhancement, are persistent throughout a year except winter, their contribution to the annual NPP would be $\sim 8\%$ ($= 51\% \times 0.20 \times 0.75$), a half of $\sim 16\%$ higher NPP in the SWES than in the southeastern part of the East Sea (Yamada et al., 2005). For the calculation, it was assumed that the NPP in the SWES is close to the annual average NPP in the UB ($0.77 \text{ g C m}^{-2} \text{ d}^{-1}$; Joo et al., 2014). The $\sim 8\%$ contribution is likely to be close to the upper bound given the fact that the CU observed in this study is one of the most noticeable events in terms of the area of the adjusted SST anomaly. The upwelled waters fraction of 20% is about twice of the mean fraction of upwelled waters found in summers (June to August) of 2003–2017. In many of modest events, NPP increase in upwelled waters should be $< 51\%$ observed in this study. Similarly, NCP in the upwelled waters were at least 70% higher than that in the ambient waters (> 0.63 vs. $0.37 \text{ g C m}^{-2} \text{ d}^{-1}$) given that the average value for the upwelled waters is likely a lower bound.

The *f*-ratio, defined as the ratio of new production over NPP (Dugdale and Goering, 1967), is known to be a measure of biological pump. Generally, it is expected that *f*-ratios in upwelling regions are somewhat higher than those in stratified regions because of higher input of ‘newly available nitrogen’ (in the form of nitrate) to the surface layer (Dugdale and Goering, 1967). Assuming that NCP approximates new production at a steady state (Falkowski et al., 2003), we calculated *f*-ratios as the ratio of gridded-NCP to satellite-NPP (Fig. 4c). The average *f*-ratios were $> 0.34 \pm 0.32$ and 0.38 ± 0.27 in the upwelled and ambient waters, respectively. Note the average for upwelled waters should be considered as a lower bound. These averages are in the range of the values predicted by some of the empirical equations relating *f*-ratios to satellite-derived SST and NPP. For example, the equation of Laws et al. (2011) predicts *f*-ratios in the range of 0.21 ± 0.03 and 0.16 ± 0.02 in the upwelled and ambient waters, respectively. The equation of Dunne et al. (2005) predicts a bit higher *f*-ratios in the range of 0.49 ± 0.03 and 0.43 ± 0.03 for the upwelled and ambient waters, respectively. However, the spatial variation of *f*-ratios predicted by the empirical equations, shown in standard deviations around 0.03, were much smaller than that of NCP/NPP ratios of ~ 0.3 (Fig. 4c). On the other hand, large variability in *f*-ratios of 0.16–0.89, similar to our observations, was observed in an *in situ* observation in the UB (Kwak et al., 2013a). Kwak et al. (2013a) used ^{15}N incubation method and attributed their highest *f*-ratio of 0.89 found near Gampo-Ulgi region to a coastal upwelling.

While most of NCPs in the ambient waters

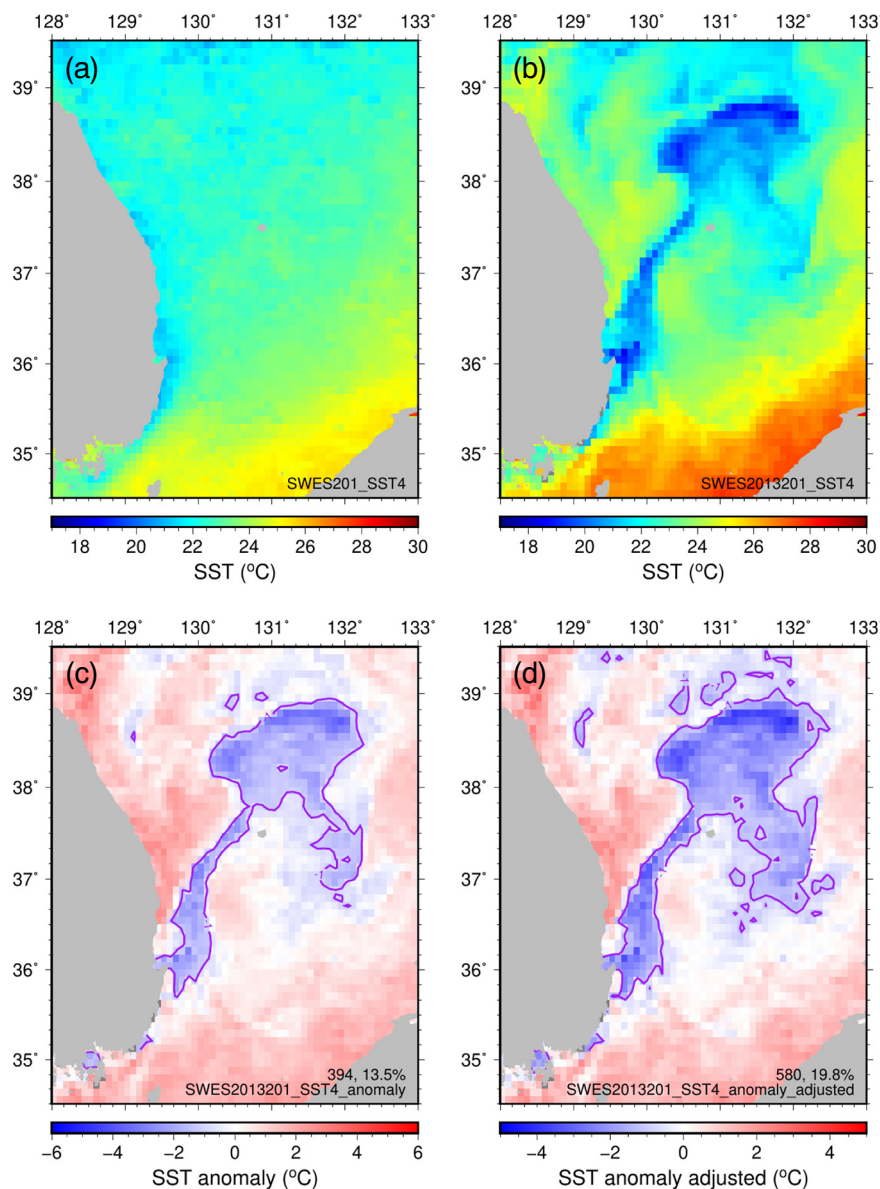


Fig. 3. The distributions of (a) average SSTs between days 201–208 in 2003–2017, (b) SSTs between days 201–208 in 2013, (c) SST anomalies in 2013, and (d) adjusted SST anomalies in 2013 (see Section 3.4 for details). The areas within purple contour lines (adjusted SST anomalies < -1 °C) are defined as upwelled waters. (For interpretation of the references to color in this figure legend, the reader is referred to the web version of this article.)

Table 2

Water properties of the upwelled and ambient waters in the SWES (gridded *in situ* and satellite data).

	Upwelled	Ambient
<i>In situ</i> SST (°C)	20.4 ± 2.0 (n = 91)	22.8 ± 1.5 (n = 266)
Satellite SST (°C)	21.2 ± 0.9 (n = 560)	24.0 ± 1.5 (n = 2286)
<i>In situ</i> Chl- <i>a</i> fluorescence	0.53 ± 0.60 (n = 101)	0.18 ± 0.22 (n = 266)
Satellite Chl- <i>a</i> (mg m ⁻³)	0.56 ± 0.50 (n = 540)	0.36 ± 0.33 (n = 2055)
<i>In situ</i> NCP ^a	> 0.63 ± 0.33 (n = 91) ^b	0.37 ± 0.18 (n = 295)
Satellite NPP ^a	1.25 ± 0.62 (n = 540)	0.83 ± 0.38 (n = 2187)
NCP/NPP (<i>f</i> -ratio)	> 0.34 ± 0.32 (n = 88) ^b	0.38 ± 0.27 (n = 282)

^a Unit: gCm⁻²d⁻¹.

^b Lower bound. See Section 3.2 for the explanation.

were < 50 mmol O₂ m⁻² d⁻¹, the area centered at 36° 20'N and 130° 50'E had NCPs > 60 mmol O₂ m⁻² d⁻¹. Because of low NPPs there, the elevated NCPs resulted in high *f*-ratios of > 0.6 (marked as a circle in

Fig. 4). The waters, observed on July 24, exhibited relatively high temperature and salinity and low Chl-*a* fluorescence. On that day, exceptionally strong winds (> 13 m s⁻¹) blew over the waters. The strong winds resulted in much higher *k_w* on July 24 (*k_w* > 25 cm h⁻¹) than the rest of the observation period. The high *k_w* indicates that Δ(O₂/Ar) has been effectively transferred from the surface waters to the atmosphere, explaining a modest increase of Δ(O₂/Ar) (< 8%). The resultant flux of [O₂]_{bio} was manifested as a prominent peak on July 24. The magnitude of the peak was comparable to those of the upwelled waters on 22 and 23 of July (Fig. 2e).

These high NCP waters may have been a part of the upwelled waters. Fig. 5, based on the outputs of the HYbrid Coordinate Ocean Model (Chassignet et al., 2007), a global data assimilation system, shows the average water temperature and currents at a depth of 10 m during the observation period. The figure suggests that cold waters upwell at the coast and travel northeastward off the coast. This is broadly consistent with the satellite observation shown in Fig. 1. Additionally, the model results indicate that some of the upwelled waters meander to the south and form a cyclonic eddy. This may be related to Dok Cold Eddy

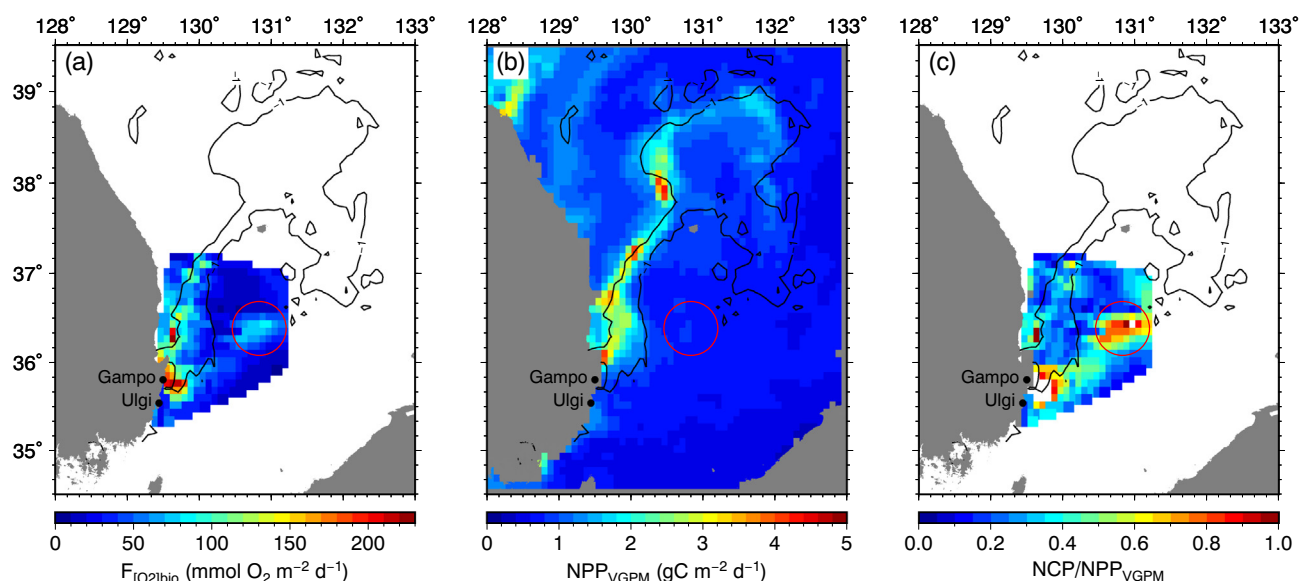


Fig. 4. The distributions of (a) gridded $[O_2]_{bio}$ flux (equivalent to NCP for the ambient waters), (b) VGPM-NPP, and (c) NCP/NPP (*f*-ratio). The black contour line shows the boundary between the upwelled and ambient waters. The red circle in each map shows the area of high NCP values on July 24, 2013. (For interpretation of the references to color in this figure legend, the reader is referred to the web version of this article.)

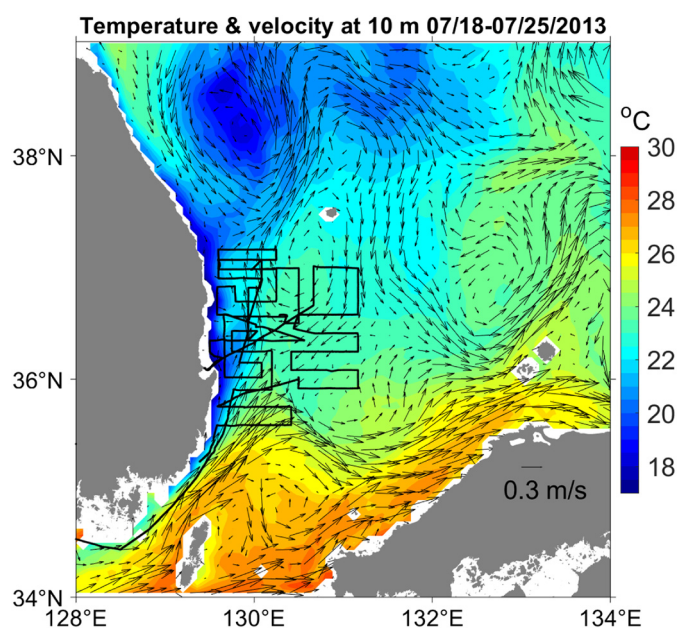


Fig. 5. Mean temperature (color) and currents (arrows) at 10 m depth obtained from HYbrid Coordinate Ocean Model in July 18–25, 2013. (For interpretation of the references to color in this figure legend, the reader is referred to the web version of this article.)

(Mitchell et al., 2005). This eddy-like water, originally upwelled at the coast, may have been a ground of high NPP during its travel to off the coast. The high SST and low Chl-*a* fluorescence of the waters are somewhat puzzling given its origin from upwelling. The surface water may have been heated and run out of nutrients during its meandering. Thus, it may not have been able to support a substantial mass of phytoplankton anymore at the time of the observation.

Alternatively, the increased NCP might be partly related to the subsurface maxima of NPP in the UB in summer (Kwak et al., 2013a). Because the NPP maxima were often observed near the bottom of the surface mixed layer, Kwak et al. (2013a) argued that satellite-based estimates, highly dependent on the SST and Chl-*a* concentration, could underestimate NPP in the UB especially in summer. Similarly, because

O_2/Ar methods represent average NCP in the mixed layer (Cassar et al., 2011; Nicholson et al., 2008), the methods will not include the fraction of NCP that occurs below the mixed layer. Ekman upwelling, resulting from the strong winds on July 24, may have brought some of the subsurface $[O_2]_{bio}$ to the surface, shown as a modest increase of $\Delta(O_2/Ar)$ ($< 8\%$). We admit that the above interpretation is circumstantial. However, we note that this yet unidentified process may play an important role in enhancing NPP and flux of sinking particles in the SWES. This process needs to be better understood by water column observations of $\Delta O_2/Ar$, Chl-*a*, and nutrients.

4. Concluding remarks

For the first time, we reported high spatial resolution observations of SST, salinity, Chl-*a* fluorescence, and NCP, capturing the physical and biogeochemical nature of the upwelled waters in the SWES. The observations and satellite data indicated that NPP were enhanced by 51% in the upwelled waters. In order to estimate overall contribution of the coastal upwelling process to the primary production in the SWES, it will be necessary to extend the area and seasonal coverage of the observation.

Because of potential upward input of low O_2 waters, NCPs in the upwelled waters were not well constrained in this study. ^{18}O *in vitro* method using a membrane inlet mass spectrometer (Ferrón et al., 2016) can be a good supplement to the current underway O_2/Ar method. The ^{18}O method, based on short-term incubation of 24 h, can provide independent estimates of NCP and gross primary production (GPP) even in the upwelled waters. Additionally, this method will provide a way to determine relative proportion of NCP and GPP both in the mixed and subsurface layers in the SWES.

Acknowledgements

We wish to thank the captain and crew of the IBRV Araon for their assistance on board. We appreciate Roberta Hamme for the constructive review. This research was supported by Basic Science Research Program through the National Research Foundation of Korea (NRF) funded by the Ministry of Education (NRF-2016R1D1A1B03931205) and by the project titled ‘Deep Water Circulation and Material Cycling in the East Sea’, funded by the Ministry of Oceans and Fisheries, Korea. T. S. Rhee

was supported by grants from Korea Polar Research Institute (PM12030 & PM18050).

Appendix A. Supplementary data

Supplementary data to this article can be found online at <https://doi.org/10.1016/j.jmarsys.2019.03.005>.

References

- Bakun, A., 1990. Global climate change and intensification of coastal ocean upwelling. *Science* 247 (4939), 198–201.
- Behrenfeld, M.J., Falkowski, P.G., 1997. Photosynthetic rates derived from satellite-based chlorophyll concentration. *Limnol. Oceanogr.* 42 (1), 1–20.
- Boyer, T.P., Antonov, J.I., Garcia, H., Johnson, D.R., Locarnini, R.A., Mishonov, A.V., et al., 2006. World Ocean Database 2005, Chapter 1: Introduction, NOAA Atlas NESDIS 60. US Government Printing Office, Washington, DC, pp. 182.
- Byun, S.-K., 1989. Sea surface cold water near the southeastern coast of Korea: wind effect. *J. Oceanol. Soc. Korea* 24, 121–131.
- Capone, D.G., Hutchins, D.A., 2013. Microbial biogeochemistry of coastal upwelling regimes in a changing ocean. *Nat. Geosci.* 6 (9), 711–717.
- Cassar, N., Barnett, B.A., Bender, M.L., Kaiser, J., Hamme, R.C., Tilbrook, B., 2009. Continuous high-frequency dissolved O_2 /Ar measurements by equilibrator inlet mass spectrometry. *Anal. Chem.* 81, 1855–1864.
- Cassar, N., DiFiore, P.J., Barnett, B.A., Bender, M.L., Bowie, A.R., Tilbrook, B., et al., 2011. The influence of iron and light on net community production in the Subantarctic and Polar Frontal Zones. *Biogeosciences* 8, 227–237.
- Chang, K.I., Teague, W.J., Lyu, S.J., Perkins, H.T., Lee, D.K., Watts, D.R., et al., 2004. Circulation and currents in the southwestern East/Japan Sea: overview and review. *Prog. Oceanogr.* 61 (2–4), 105–156.
- Chassignet, E.P., Hurlburt, H.E., Smedstad, O.M., Halliwell, G.R., Hogan, P.J., Wallcraft, A.J., et al., 2007. The HYCOM (HYbrid Coordinate Ocean model) data assimilative system. *J. Mar. Syst.* 65 (1–4), 60–83.
- Craig, H., Hayward, T., 1987. Oxygen supersaturation in the ocean: biological versus physical contributions. *Science* 235 (4785), 199–202.
- Dugdale, R., Goering, J., 1967. Uptake of new and regenerated forms of nitrogen in primary productivity. *Limnol. Oceanogr.* 196–206.
- Dunne, J., Armstrong, R., Gnanadesikan, A., Sarmiento, J., Slater, R., 2005. Empirical and mechanistic models for the particle export ratio. *Glob. Biogeochem. Cycles* 19.
- Emerson, S.R., Hedges, J., 2008. *Chemical Oceanography and the Marine Carbon Cycle*. Cambridge University Press, pp. 1–468.
- Falkowski, P.G., Laws, E.A., Barber, R.T., Murray, J.W., 2003. Phytoplankton and their role in primary, new, and export production. In: *Ocean Biogeochemistry*. Springer, pp. 99–121.
- Ferrón, S., del Valle, D.A., Björkman, K.M., Quay, P.D., Church, M.J., Karl, D.M., 2016. Application of membrane inlet mass spectrometry to measure aquatic gross primary production by the $18O$ in vitro method. *Limnol. Oceanogr. Methods* 1–13.
- Garcia, H., Gordon, L., 1992. Oxygen solubility in seawater: better fitting equations. 37 (6), 1307–1312.
- Giesbrecht, K.E., Hamme, R.C., Emerson, S.R., 2012. Biological productivity along Line P in the subarctic northeast Pacific: in situ versus incubation-based methods. *Glob. Biogeochem. Cycles* 26 (3), GB3028.
- Hahn, D., Rhee, T.S., Kim, H.-C., Park, J., Kim, Y.N., Shin, H.C., Lee, S., 2014. Spatial and temporal variation of net community production and its regulating factors in the Amundsen Sea, Antarctica. *J. Geophys. Res.* 119 (5), 2815–2826.
- Hamme, R.C., Emerson, S.R., 2004. The solubility of neon, nitrogen and argon in distilled water and seawater. *Deep-Sea Res. I* 51 (11), 1517–1528.
- Haskell, W.Z., Prokopenko, M.G., Stanley, R.H.R., Knapp, A.N., 2016. Estimates of vertical turbulent mixing used to determine a vertical gradient in net and gross oxygen production in the oligotrophic South Pacific Gyre. *Geophys. Res. Lett.* 43 (14), 7590–7599.
- Haskell, W.Z., Prokopenko, M.G., Hammond, D.E., Stanley, R.H.R., Sandwith, Z.O., 2017. Annual cyclicity in export efficiency in the inner Southern California Bight. *Glob. Biogeochem. Cycles* 31 (2), 357–376.
- Hyun, J., Kim, D., Shin, C., Noh, J., Yang, E., Mok, J., et al., 2009. Enhanced phytoplankton and bacterioplankton production coupled to coastal upwelling and an anticyclonic eddy in the Ulleung basin, East Sea. *Aquat. Microb. Ecol.* 54, 45–54.
- Johnson, K.S., Plant, J.N., Riser, S.C., Gilbert, D., 2015. Air oxygen calibration of oxygen optodes on a profiling float array. *J. Atmos. Ocean. Technol.* 32 (11), 2160–2172.
- Joo, H., Park, J.W., Son, S., Noh, J.-H., Jeong, J.-Y., Kwak, J.H., et al., 2014. Long-term annual primary production in the Ulleung Basin as a biological hot spot in the East/Japan Sea. *J. Geophys. Res.* 119 (5), 3002–3011.
- Juranek, L., Hamme, R., Kaiser, J., Wanninkhof, R., Quay, P., 2010. Evidence of O_2 consumption in underway seawater lines: Implications for air-sea O_2 and CO_2 fluxes. *Geophys. Res. Lett.* 37 (1), L01601.
- Kalnay, E., Kanamitsu, M., Kistler, R., Collins, W., Deaven, D., Gandin, L., et al., 1996. The NCEP/NCAR 40-year reanalysis project. *Bull. Am. Meteorol. Soc.* 77 (3), 437–471.
- Kim, D., Yang, E.J., Kim, K.H., Shin, C.W., Park, J., Yoo, S., Hyun, J.H., 2012. Impact of an anticyclonic eddy on the summer nutrient and chlorophyll a distributions in the Ulleung Basin, East Sea (Japan Sea). *ICES J. Mar. Sci.* 69 (1), 23–29.
- Kim, S.-K., Chang, K.-I., Kim, B., Cho, Y.-K., 2013. Contribution of ocean current to the increase in N abundance in the Northwestern Pacific marginal seas. *Geophys. Res. Lett.* 40 (1), 143–148.
- Kwak, J.H., Lee, S.H., Park, H.J., Choy, E.J., Jeong, H.D., Kim, K.R., Kang, C.K., 2013a. Monthly measured primary and new productivities in the Ulleung Basin as a biological “hot spot” in the East/Japan Sea. *Biogeosciences* 10 (7), 4405–4417.
- Kwak, J.H., Hwang, J., Choy, E.J., Park, H.J., Kang, D.-J., Lee, T., Chang, K.-I., Kim, K.-R., Kang, C.-K., 2013b. High primary productivity and f-ratio in summer in the Ulleung basin of the East/Japan Sea. *Deep-Sea Res. I* 79 (C), 74–85.
- Lachkar, Z., Gruber, N., 2013. Response of biological production and air-sea CO_2 fluxes to upwelling intensification in the California and Canary Current Systems. *J. Mar. Syst.* 109–110, 149–160.
- Laws, E.A., 1991. Photosynthetic quotients, new production and net community production in the open ocean. *Deep-Sea Res.* 38 (1), 143–167.
- Laws, E.A., D'Sa, E., Naik, P., 2011. Simple equations to estimate ratios of new or export production to total production from satellite-derived estimates of sea surface temperature and primary production. *Limnol. Oceanogr. Methods* 9, 593–601.
- Lee, J.C., 1983. Variations of sea level and sea surface temperature associated with wind-induced upwelling in the southeast coast of Korea in summer. *J. Oceanol. Soc. Korea* 18 (2), 149–160.
- Lee, J.C., Na, J.Y., 1985. Structure of upwelling off the southeast coast of Korea. *J. Oceanol. Soc. Korea* 20 (3), 6–19.
- Lee, D.-K., Niiler, P., 2010. Surface circulation in the southwestern Japan/East Sea as observed from drifters and sea surface height. *Deep-Sea Res. I* 57 (10), 1222–1232.
- Lim, S., Jang, C.J., Oh, I.S., Park, J., 2012. Climatology of the mixed layer depth in the East/Japan Sea. *J. Mar. Syst.* 96–97 (C), 1–14.
- Lockwood, D., Quay, P.D., Kavanaugh, M.T., Juranek, L.W., Feely, R.A., 2012. High-resolution estimates of net community production and air-sea CO_2 flux in the northeast Pacific. *Glob. Biogeochem. Cycles* 26 (4), GB4010.
- Manning, C.C., Stanley, R.H.R., Nicholson, D.P., Smith, J.M., Timothy Pennington, J., Fewings, M.R., et al., 2017. Impact of recently upwelled water on productivity investigated using in situ and incubation-based methods in Monterey Bay. *J. Geophys. Res. Oceans* 122 (3), 1901–1926.
- Mitchell, D.A., Watts, D.R., Wimbush, M., Teague, W.J., Tracey, K.L., Book, J.W., et al., 2005. Upper circulation patterns in the Ulleung Basin. *Deep-Sea Res. II Top. Stud. Oceanogr.* 52 (11–13), 1617–1638.
- Nicholson, D., Emerson, S., Eriksen, C.C., 2008. Net community production in the deep euphotic zone of the subtropical North Pacific gyre from glider surveys. *Limnol. Oceanogr.* 53, 2226–2236.
- Onitsuka, G., Yanagi, T., Yoon, J.-H., 2007. A numerical study on nutrient sources in the surface layer of the Japan Sea using a coupled physical-ecosystem model. *J. Geophys. Res. Oceans* 112 (C5), C05042.
- Park, K.-A., Kim, K.-R., 2010. Unprecedented coastal upwelling in the East/Japan Sea and linkage to long-term large-scale variations. *Geophys. Res. Lett.* 37 (9), L09603.
- Reuer, M., Barnett, B., Bender, M., Falkowski, P., Hendricks, M., 2007. New estimates of southern ocean biological production rates from O_2 /Ar ratios and the triple isotope composition of O_2 . *Deep-Sea Res. I* 54 (6), 951–974.
- Rho, T., Lee, T., Kim, G., Chang, K.-I., Na, T., Kim, K.-R., 2012. Prevailing Subsurface Chlorophyll Maximum (SCM) Layer in the East Sea and Its Relation to the Physico-Chemical Properties of Water Masses. *Ocean Polar Res.* 34 (4), 413–430.
- Spitzer, W.S., Jenkins, W.J., 1989. Rates of vertical mixing, gas exchange and new production: estimates from seasonal gas cycles in the upper ocean near Bermuda. *J. Mar. Res.* 47 (1), 169–196.
- Teeter, L., Hamme, R.C., Ianson, D., Bianucci, L., 2018. Accurate estimation of net community production from O_2 /Ar measurements. *Glob. Biogeochem. Cycles* 110 (5), C10S01.
- Tortell, P.D., 2005. Dissolved gas measurements in oceanic waters made by membrane inlet mass spectrometry. 3, 24–37.
- Wanninkhof, R., 1992. Relationship between wind speed and gas exchange. *J. Geophys. Res.* 97 (C5), 7373–7382.
- Yamada, K., Ishizaka, J., Nagata, H., 2005. Spatial and temporal variability of satellite primary production in the Japan Sea from 1998 to 2002. *J. Oceanogr.* 61 (5), 857–869.
- Yoo, S., Park, J., 2009. Why is the southwest the most productive region of the East Sea/Sea of Japan? *J. Mar. Syst.* 78 (2), 301–315.